

# PCCP

Accepted Manuscript



This is an *Accepted Manuscript*, which has been through the Royal Society of Chemistry peer review process and has been accepted for publication.

*Accepted Manuscripts* are published online shortly after acceptance, before technical editing, formatting and proof reading. Using this free service, authors can make their results available to the community, in citable form, before we publish the edited article. We will replace this *Accepted Manuscript* with the edited and formatted *Advance Article* as soon as it is available.

You can find more information about *Accepted Manuscripts* in the [Information for Authors](#).

Please note that technical editing may introduce minor changes to the text and/or graphics, which may alter content. The journal's standard [Terms & Conditions](#) and the [Ethical guidelines](#) still apply. In no event shall the Royal Society of Chemistry be held responsible for any errors or omissions in this *Accepted Manuscript* or any consequences arising from the use of any information it contains.

## Anisotropic thermoelectric properties of layered compounds in SnX<sub>2</sub> (X = S, Se): A promising thermoelectric

Bao-Zhen Sun,<sup>ab</sup> Zuju Ma,<sup>a</sup> Chao He<sup>a</sup> and Kechen Wu<sup>\*a</sup>

Thermoelectrics interconvert heat to electricity and are of great interest in waste heat recovery, solid-state cooling and so on. Here we assessed the potential of SnS<sub>2</sub> and SnSe<sub>2</sub> as a thermoelectric material at the temperature gradient from 300 to 800 K. Reflecting the crystal structure, the transport coefficients are highly anisotropic between *a* and *c* directions, in particular for the electrical conductivity. The preferred direction for both materials is *a* direction in TE application. Most strikingly, when 800 K is reached, SnS<sub>2</sub> can show a peak power factor (*PF*) of 15.50 μW·cm<sup>-1</sup>·K<sup>-2</sup> along the *a* direction, while a relatively lower value (11.72 μW·cm<sup>-1</sup>·K<sup>-2</sup>) is obtained in the same direction of SnSe<sub>2</sub>. These values are comparable to those observed in thermoelectrics such as SnSe and SnS. At 300 K, the minimum lattice thermal conductivity ( $\kappa_{\min}$ ) along the *a* direction is estimated to be about 0.67 and 0.55 W·m<sup>-1</sup>·K<sup>-1</sup> for SnS<sub>2</sub> and SnSe<sub>2</sub>, respectively, even lower than the measured lattice thermal conductivity of Bi<sub>2</sub>Te<sub>3</sub> (1.28 W·m<sup>-1</sup>·K<sup>-1</sup> at 300 K). The reasonable *PF* and  $\kappa_{\min}$  suggest that both SnS<sub>2</sub> and SnSe<sub>2</sub> are potential thermoelectric materials. Indeed, the estimated peak *ZT* can approach 0.88 for SnSe<sub>2</sub> and a higher value of 0.96 for SnS<sub>2</sub> along the *a* direction at a carrier concentration of 1.94×10<sup>19</sup> (SnSe<sub>2</sub>) vs. 2.87×10<sup>19</sup> cm<sup>-3</sup> (SnS<sub>2</sub>). The best *ZT* values in SnX<sub>2</sub> (X = S, Se) are comparable to that in Bi<sub>2</sub>Te<sub>3</sub> (0.8), a typical thermoelectric material. We hope this theoretical investigation will

<sup>a</sup> State Key Laboratory of Structural Chemistry, Fujian Institute of Research on the Structure of Matter, Chinese Academy of Science, Fuzhou 350002, China. E-mail: wkc@fjirsm.ac.cn

<sup>b</sup> School of Chemistry and Chemical Engineering, Guangxi University, Nanning 530004, China

provide useful information for further experimental and theoretical studies on optimizing the thermoelectric properties of  $\text{SnX}_2$  materials.

## 1 Introduction

2 The use of thermoelectric (TE) materials to harvest electricity from waste heat via the  
3 Seebeck effect has become increasingly important, because of the global need for  
4 energy production and conservation.<sup>1-3</sup> The TE efficiency of a material used in TE  
5 devices is determined by the dimensionless figure of merit,  $ZT = S^2\sigma T/\kappa$ , where  $S$  is  
6 the Seebeck coefficient or thermopower,  $\sigma$  the electrical conductivity,  $T$  the absolute  
7 temperature, and  $\kappa$  the thermal conductivity ( $\kappa = \kappa_L + \kappa_E$ , where  $\kappa_L$  and  $\kappa_E$  are the  
8 lattice and electronic contributions, respectively). By definition, we see that a large  
9 Seebeck coefficient, a high electrical conductivity, and a low thermal conductivity are  
10 needed to achieve a high  $ZT$ . In the past few years, pursuing high  $ZT$  has been the  
11 focus of TE studies. However, for practical applications, efficiency is not the only  
12 concern, and toxicity, price and density of the material are issues that must also be  
13 taken into account. Thus, one of the current main interests is to develop new,  
14 non-toxic and cheap thermoelectric materials.

15 Because of their anisotropic character, layered compounds appear to be attractive  
16 targets in the quest for TE materials. Indeed, some of them (for example  $A_2^V B_3^{VI}$ ,<sup>4-6</sup>  
17  $A^{IV} B^{VI}$ ,<sup>7-10</sup> and layered Co oxides<sup>11-13</sup>) display interesting thermoelectric properties.  
18 This holds especially true for SnSe which exhibits an outstanding  $ZT$  value of  $\sim 2.6$  at  
19 923 K.<sup>7</sup> This is also well evidenced in the layered  $Bi_2Te_3$ -based materials which are  
20 the best TE materials around room temperature.<sup>14</sup> In layered structure, an interesting  
21 feature is that the layer and the interlayer spacing can often be modified independently,

1 and hence leading to the possibility of tuning the electronic and thermal transport  
2 properties adequately. This is an advantageous situation for thermoelectrics. What's  
3 more, the bonds between the layers are extremely weak (due to weak van der Waal's  
4 forces). It is beneficial to the low thermal conductivity. For instance, this has been  
5 proven in the layered compounds such as  $(\text{Na}, \text{Ca})\text{Co}_2\text{O}_4$ ,<sup>15</sup>  $\text{AgCrSe}_2$ ,<sup>16</sup> and  $\text{SnSe}$ .<sup>7,17</sup>  
6 For these reasons, the TE potential of layered metal dichalcogenides  $\text{MX}_2$  (M is a  
7 metal atom like Sn, Ti, Zr, or Hf and X is a chalcogen like S, Se, or Te) has  
8 increasingly attracted attention.

9 The family of  $\text{MX}_2$  have been investigated for a long period and are known to  
10 exhibit several interesting physical properties as well as find innovative practical  
11 applications, such as solid lubricant, photovoltaics, electrochemical fuel cells, etc.<sup>18-20</sup>  
12  $\text{MX}_2$  compounds typically grow in layered crystals similar to graphite and the  
13 interaction between the layers is weak van der Waals type and, therefore, they can be  
14 easily intercalated by various guest species. This will greatly affect their structural and  
15 electronic properties, which in turn means that the TE properties of these materials  
16 can be optimized by controlling the type and the concentration of the dopants.<sup>21</sup>  
17 Recently, several studies have demonstrated the great TE potential of  $\text{MX}_2$   
18 compounds.<sup>16, 22-24</sup> Typical examples include the dichalcogenides  $\text{MX}_2$  (M = Mo, W,  
19 Ti; X = S, Se, Te), which are good candidates for thermoelectric applications because  
20 of their high Seebeck coefficients and low thermal conductivity.<sup>23, 25, 26</sup> For example,  
21 Guilmeau E. *et al.*<sup>24</sup> reported that  $\text{TiS}_2$  exhibits high power factor value of 1.7  
22  $\text{mW}\cdot\text{m}^{-1}\cdot\text{K}^{-2}$  at 325 K. Most recently, Nunna R. *et al.*<sup>27</sup> further proposed that the ZT

1 value increases with temperature and reaches a maximum value of 0.54 at 700 K for  
2  $\text{Cu}_{0.05}\text{TiS}_{1.5}\text{Se}_{0.5}$ , the highest value so far observed in layered titanium chalcogenides.  
3 Naidu A. *et al.*<sup>28</sup> also interestingly found that  $\text{WS}_2$  is an excellent high-temperature  
4 thermoelectric material. The maximal  $ZT$  values of 0.90 and 0.77 for  $n$ -type and  
5  $p$ -type  $\text{WS}_2$ , respectively, are obtained at 1500 K and are comparable to the best  
6 thermoelectric materials currently used in devices.<sup>29</sup> Further enhancement to  $ZT$  is  
7 anticipated for these materials in future research.

8  $\text{SnS}_2$  and  $\text{SnSe}_2$  are another interesting  $\text{MX}_2$  compounds, and both crystallize in  
9 hexagonal close-packed  $\text{CdI}_2$ -type layered structure, hence, it may be of interest to  
10 study the TE properties of  $\text{SnS}_2$  and  $\text{SnSe}_2$ . In addition,  $\text{SnS}_2$  and  $\text{SnSe}_2$  offer several  
11 advantages for practical applications, such as non-toxicity, low cost. However, only  
12 limited information is now available concerning the TE properties of  $\text{SnS}_2$  and  
13  $\text{SnSe}_2$ .<sup>30, 31</sup> The optimal temperature and doping concentration have not been  
14 determined experimentally and theoretically. In either case, thermal conductivity data  
15 are lacking because of difficulties in the handling the lattice thermal conductivity. To  
16 access the potential of  $\text{SnS}_2$  and  $\text{SnSe}_2$  as a thermoelectric material, in this work, we  
17 theoretically examine the doping and temperature dependence of TE properties of  
18  $\text{SnX}_2$  ( $X=\text{S}, \text{Se}$ ) by using first-principles band structure calculations and Boltzmann  
19 transport theory.<sup>32</sup> In particular, the anisotropy of transport coefficients is discussed  
20 and the lattice thermal conductivity is evaluated using the approach developed by  
21 Cahill.<sup>33</sup> Our results may serve as a guide on how to optimize the thermoelectric  
22 properties of these compounds.

## 1 Computational detail

2 Density functional theory (DFT) based on the Vienna ab-initio Simulation Package  
3 (VASP)<sup>34</sup> is used with plane wave energy up to 400 eV in the expansion of the  
4 electronic wave function. For the structure optimization and the electronic structure  
5 calculations we employ the Heyd-Scuseria-Ernzerhof (HSE03) hybrid functional.<sup>35</sup>  
6 This methodology has been shown to provide good band structure predictions. The  
7 valence electron configurations considered in this calculation are Sn(4d<sup>10</sup>5s<sup>2</sup>5p<sup>2</sup>),  
8 S(3s<sup>2</sup>3p<sup>4</sup>), and Se(4s<sup>2</sup>4p<sup>4</sup>), respectively. The lattice vectors and atomic positions are  
9 fully relaxed by minimizing the quantum mechanical stresses and forces. The  
10 convergence for energy is chosen as 10<sup>-6</sup> eV between two steps. The structural  
11 optimization is obtained until the Hellman-Feynman forces acting on each atom are  
12 less than 0.01 eV/Å. A Monkhorst-Pack k-point mesh of 6×6×4 are used to sample the  
13 Brillouin zones in the structural optimization and self-consistent calculation.

14 Transport calculations are performed through solving the Boltzmann Transport  
15 Equations within the rigid band and constant relaxation-time ( $\tau$ ) approximations as  
16 implemented in BOLTZTRAP program.<sup>32</sup> Rigid band approximation (RBA) is the  
17 assumption that the band structure of the host is unchanged by doping, only the  
18 chemical potential changes with doping concentration and of course temperature.  
19 RBA usually overestimates the Seebeck coefficient and the power factor.<sup>36</sup> The  
20 constant relaxation-time approximation assumes  $\tau$  as energy-independent. The  
21 advantage of using this approximation is that the Seebeck coefficient can be  
22 calculated without adjustable parameters.  $\tau$  has a complex  $T$  dependence depending

1 on the scattering mechanism. Sources of scattering in semiconductors are ionized  
2 impurities, neutral impurities, and electron-phonon interaction (acoustic phonon  
3 scattering, optical phonon scattering, and piezoelectric scattering), etc.  $\tau$  is directly  
4 proportional to the temperature in ionized impurity scattering whereas independent of  
5 the temperature in neutral impurity scattering.  $\tau$  will decrease with temperature if the  
6 scattering is dominated by an electron-phonon interaction (the primary scattering  
7 mechanism in heavily doped semiconductors). In Boltzmann method, all kinds of  
8 scattering processes can be simply introduced by relaxation time approximation. Its  
9 prime advantage is that detailed assumptions about the nature of the scattering are not  
10 necessary. The calculation of  $\tau$  is a very difficult task. Typically,  $\tau$  is treated as a  
11 constant for simplicity and convenience.<sup>37-39</sup> Choosing a constant for  $\tau$  is an  
12 approximation for the real scattering mechanism. This approximation might result in  
13 the overestimations in the electrical conductivity and therefore in  $ZT$  predictions. It is  
14 difficult to reliably predict the temperature dependence of transport coefficients under  
15 this assumption. However to obtain the electrical conductivity and  $ZT$  the constant  
16 relaxation-time approximation is more feasible. Nevertheless, this *ab initio* approach  
17 has been successfully used in rationalizing and predicting the optimal doping level of  
18 known compounds and recently has been used to screen potential candidates for TE  
19 materials.

20 A more dense  $k$ -point grid of  $12 \times 12 \times 8$  is used for transport calculations to  
21 guarantee convergence and to obtain accurate carrier group velocities, which are  
22 essential for determining the transport properties.  $ZT$  can be evaluated by

$$ZT = \frac{S^2 \sigma T}{\kappa_E + \kappa_L} = \frac{S^2}{L_0 + \frac{\kappa_L}{\sigma T}} \quad (1)$$

where  $L_0 = 2.45 \times 10^{-8} \text{ W} \cdot \Omega \cdot \text{K}^{-2}$  is the Lorentz number. Here,  $\kappa_L$  adopted the value of the minimum lattice thermal conductivity, which can be calculated by Cahill's model<sup>33</sup>:

$$\kappa_{\min} = \left(\frac{\pi}{6}\right)^{1/3} \kappa_B n^{2/3} \sum_i v_i \left(\frac{T}{\Theta_i}\right)^2 \int_0^{\Theta_i/T} \frac{x^3 e^x}{(e^x - 1)^2} dx \quad (2)$$

where  $v$ ,  $\Theta$  and  $n$  are the phonon velocity, Debye temperature and the number density of atoms, respectively. The values of  $v$  and  $\Theta$  are calculated from the phonon dispersion. This approach has been successfully applied to estimate the  $\kappa_{\min}$  of several materials, such as SnSe<sup>7</sup>, SrTiO<sub>3</sub><sup>40</sup>, In<sub>2</sub>O<sub>3</sub>-based compounds<sup>41</sup>.

Phonon dispersion is calculated using the supercell (192 atoms in the SnS<sub>2</sub> supercell and 240 atoms in the SnSe<sub>2</sub> supercell) force constant method. The harmonic second order interatomic force constants (IFCs) were obtained within the linear response framework by employing the density functional perturbation theory (DFPT)<sup>42</sup> as implemented in the VASP code. Then we could get the phonon dispersion of SnS<sub>2</sub> and SnSe<sub>2</sub> using the PHONOPY package<sup>43</sup> based on the harmonic second order IFCs.

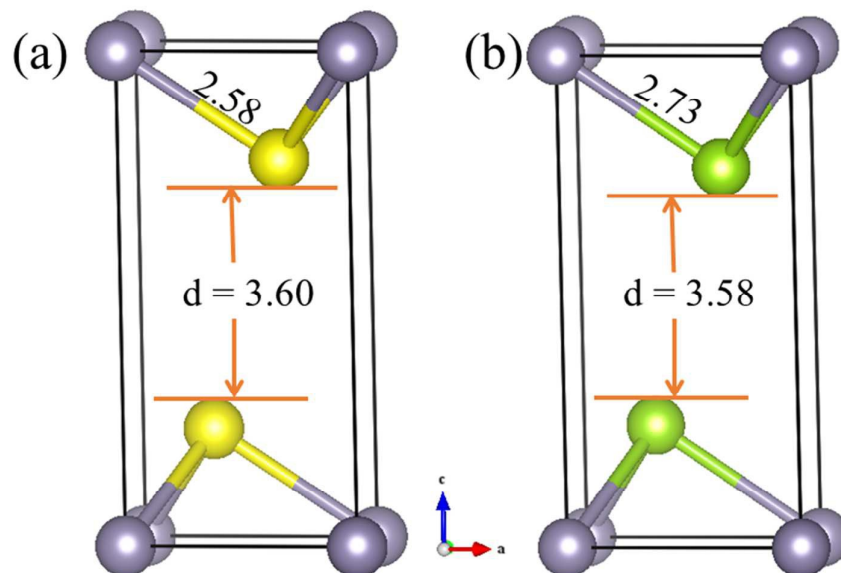
## 17 Results and discussion

### 18 3.1 Geometrical structure

19 SnS<sub>2</sub> and SnSe<sub>2</sub> often crystallize in different polytypes. The usual and stable polytype

1 is 2H, *i.e.* a hexagonal unit cell consisting of two layers.<sup>44</sup> Therefore, type 2H was  
2 chosen to model the SnX<sub>2</sub> (X =S, Se) crystals in our calculations. It has an anisotropic  
3 structure with a trigonal space group,  $P\bar{3}m1$ . Within one layer, a plane of Sn atoms is  
4 sandwiched between two S/Se planes with strong covalent metal-anion bonds in the  
5 *a-b* plane. The formed S(Se)-Sn-S(Se) layers are stacked by weak van der Waals  
6 interactions along the *c* axis. Fig. 1 shows the optimized SnX<sub>2</sub> structures. In the  
7 crystal structure of SnX<sub>2</sub>, Sn atoms occupy the 1a (0 0 0) site, S atoms at 2d (0.333  
8 0.667 0.224) site, and Se atoms at the 2d (0.333 0.667 0.234) site. The bond length of  
9 Sn-S vs. Sn-Se is calculated to be 2.58 vs. 2.73 Å, which matches the corresponding  
10 experimental value (2.57 vs. 2.69 Å)<sup>45</sup>. Clearly, the Sn-S bond length is smaller than  
11 that of Sn-Se, as S has a smaller atomic radius. It brings about the corresponding  
12 weaker intra-layer bonding for SnSe<sub>2</sub>. As is known, weaker bonding leads to lower  
13 thermal conductivity.<sup>46</sup> Thus, lower thermal conductivity along the *a* axis could be  
14 anticipated for SnSe<sub>2</sub>. In addition, the optimized interlayer separations for SnS<sub>2</sub> and  
15 SnSe<sub>2</sub> are approximately identical and significantly exceeds 3 Å, suggestive of weak  
16 bonding and hence soft phonons, favorable for TE performance.

17



1

2 **Fig. 1** Crystal structures of SnX<sub>2</sub> (space group *P-3m1*). (a) SnS<sub>2</sub>; (b) SnSe<sub>2</sub>. The unit of  
3 interatomic distance is in Å. Here, grey, yellow and green colors represent Sn, S and  
4 Se atoms, respectively.

5

### 6 **3.2 Electronic structure**

7 To study the TE properties, an accurate electronic structure is required. We calculated  
8 the band gap of SnS<sub>2</sub> and SnSe<sub>2</sub> with PBE, HSE03, and HSE06 functionals, listed in  
9 Table 1. From the PBE calculations, SnS<sub>2</sub> (SnSe<sub>2</sub>) is found to have an indirect band  
10 gap of 1.55 (0.71) eV. However, the band gap calculated through the HSE03  
11 functional is found to be 2.04 (1.09) eV, which is closer to the experimental value<sup>47</sup>  
12 compared with the corresponding gap from HSE06 functional (2.53 and 1.48 eV,  
13 respectively). Hence, here onward we will discuss only the HSE03 results. The band  
14 dispersion plots of SnS<sub>2</sub> and SnSe<sub>2</sub> calculated through the HSE03 method are shown  
15 in Fig. S1. The band gap for SnSe<sub>2</sub> is smaller than that for SnS<sub>2</sub>, which is consistent  
16 with our common expectation that the selenides have smaller band gaps than the

1 corresponding sulfides.

2

3 **Table 1** Calculated band gap results of SnX<sub>2</sub> (X = S, Se) systems using PBE, HSE03,  
4 and HSE06 methods

System	band gap (eV)			Expt.
	PBE	HSE03	HSE06	
SnS <sub>2</sub>	1.55	2.04	2.53	2.07 (ref. 47)
SnSe <sub>2</sub>	0.71	1.09	1.48	0.97 (ref. 47)

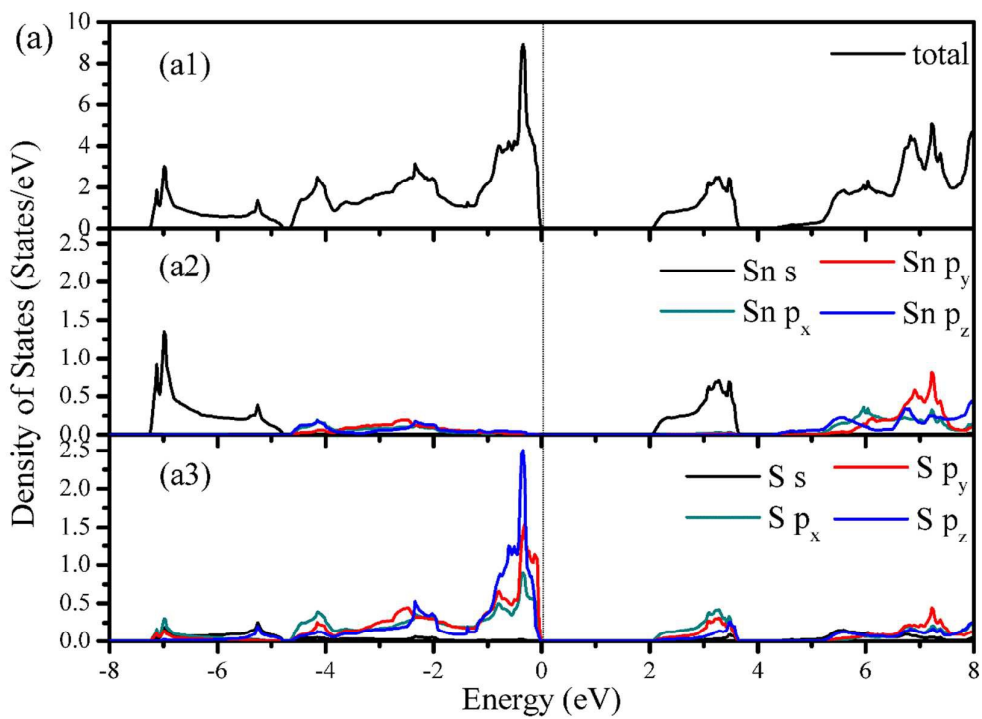
5

6 In addition, we also calculated the electron effective masses ( $m^*$ ) for SnS<sub>2</sub> and SnSe<sub>2</sub>  
7 in two different directions of the reciprocal space by fitting the band structure around  
8 the CBM using the equation  $m^* = \hbar^2 / (d^2E/dk^2)$ . In the  $G \rightarrow A$  direction ( $c$  axis),  
9 the calculated effective masses are  $0.43 m_0$  ( $m_0$  is the electron mass) for SnS<sub>2</sub> and  $0.28$   
10  $m_0$  for SnSe<sub>2</sub>, while in the  $G \rightarrow K$  direction ( $a$  axis), values of  $0.61 m_0$  and  $0.52 m_0$   
11 were found for SnS<sub>2</sub> and SnSe<sub>2</sub>, respectively. The electron effective mass of SnSe<sub>2</sub>  
12 along the  $a$  axis is estimated as  $0.4 \pm 0.2 m_0$  by Lee *et al.*,<sup>48</sup> in agreement with our  
13 predicted value for SnSe<sub>2</sub> in the  $a$  direction. A high effective mass translates to larger  
14 Seebeck coefficient. For both materials, the higher value for  $m^*$  in the  $G \rightarrow K$   
15 direction compared to that in the  $G \rightarrow A$  direction indicates improved Seebeck  
16 coefficient from  $c$  to  $a$  direction. Likewise, in both directions, the Seebeck coefficient  
17 can be increased by replacing Se by S.

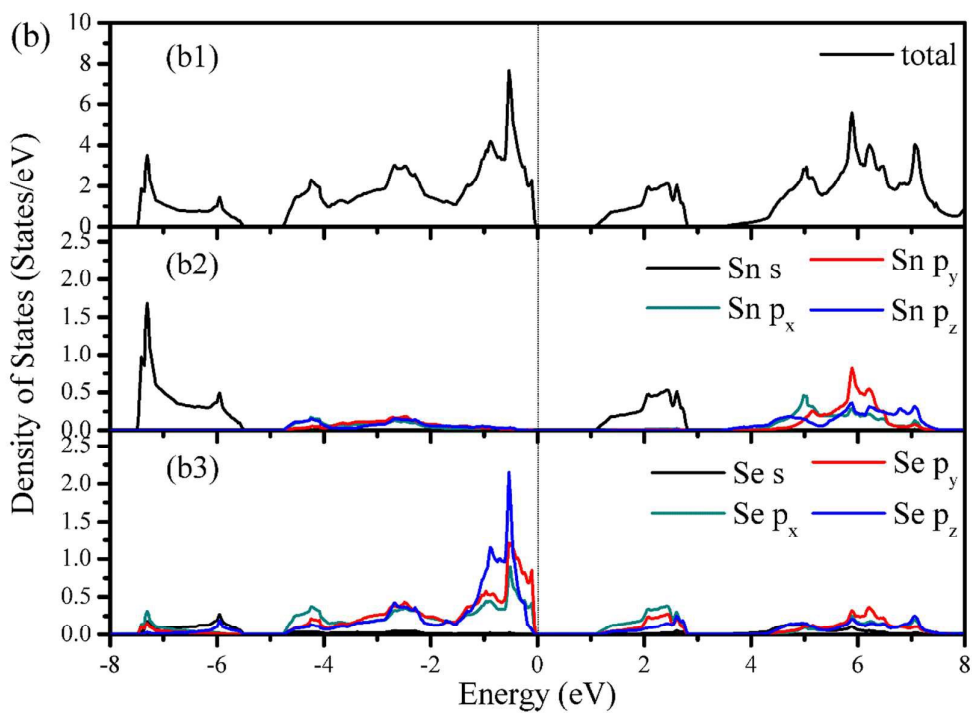
18 Since the electron states around the Fermi level have an important effect on the  
19 TE transport properties of SnS<sub>2</sub> and SnSe<sub>2</sub>, we calculated their total and partial density  
20 of states (TDOS and PDOS) and draw them in Fig. 2. Due to the similar crystalline  
21 structure and bonding nature, the total DOS of SnS<sub>2</sub> and SnSe<sub>2</sub> has similar shape.

1 From Fig. 2(a1) and (b1), we can see that the conduction band (CB) is much  
2 delocalized than the valence band (VB) near the Fermi level, which is indicative of a  
3 higher electrical conductivity for *n*-type doping. Moreover, experimental studies<sup>47-50</sup>  
4 revealed that both SnS<sub>2</sub> and SnSe<sub>2</sub> usually exhibit *n*-type conduction and so only  
5 *n*-type doping was considered in the following TE properties. From the partial DOS, it  
6 is found that for both compounds the VB from -5 eV to Fermi level is composed of p  
7 orbital of the chalcogen (S or Se), while the CB near the Fermi level is mainly  
8 dominated by Sn 5s state and chalcogen p states. This means the electrical  
9 conductivity and Seebeck coefficient for *n*-type are primarily determined by Sn 5s and  
10 chalcogen p electrons. Generally, large Seebeck coefficients are usually associated  
11 with a large DOS peak. As seen in Fig. 2, moving from SnS<sub>2</sub> to SnSe<sub>2</sub>, the peaks  
12 becomes lower in the CB near Fermi level, which will make the Seebeck coefficient  
13 decrease from SnS<sub>2</sub> to SnSe<sub>2</sub> for *n*-type doping. In the CB of both materials, we also  
14 note the increase of the chalcogen p-orbital contribution from p<sub>z</sub> to p<sub>x</sub>, which is  
15 probably related to the increase in the Seebeck coefficient from p<sub>z</sub> to p<sub>x</sub>. In other  
16 words, *a* direction has a higher Seebeck coefficient than *c* direction for *n*-type doping  
17 of both materials. These observations support the above results obtained by analyzing  
18 electron effective mass. We will observe these points in the following section.

19



1



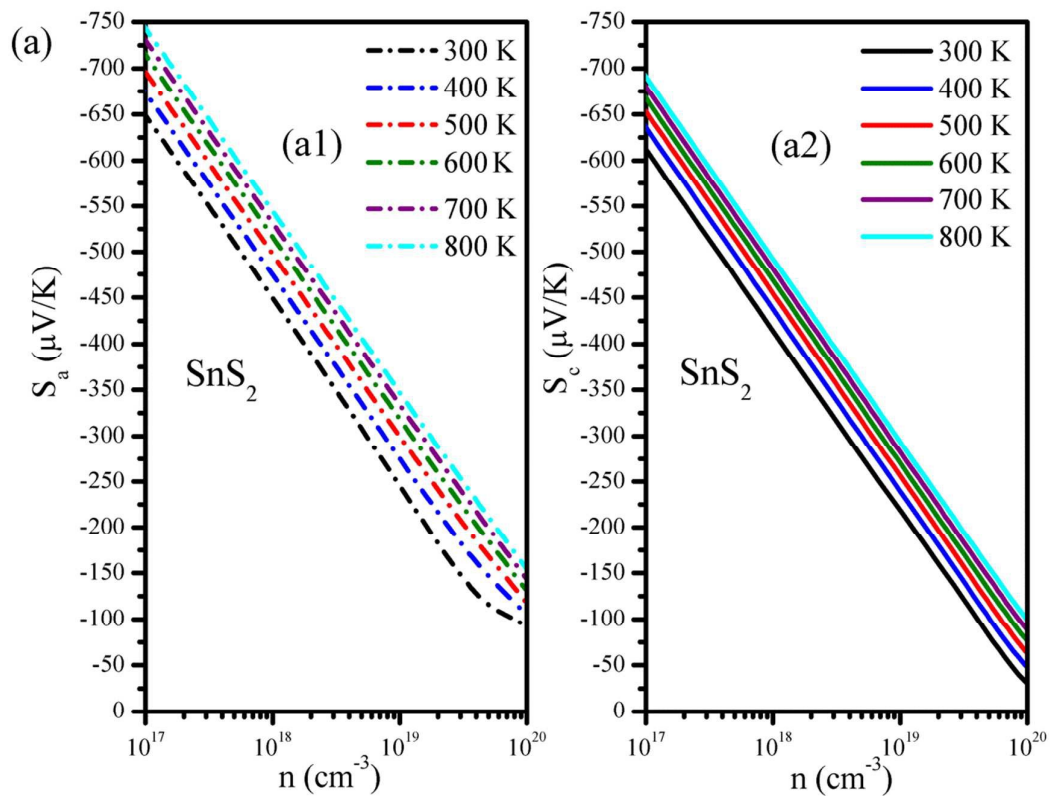
2

3 **Fig. 2** Calculated total DOS and partial DOS for (a) SnS<sub>2</sub> and (b) SnSe<sub>2</sub> within the  
 4 energy range -8 to 8 eV. Top of the valence band is set to zero.

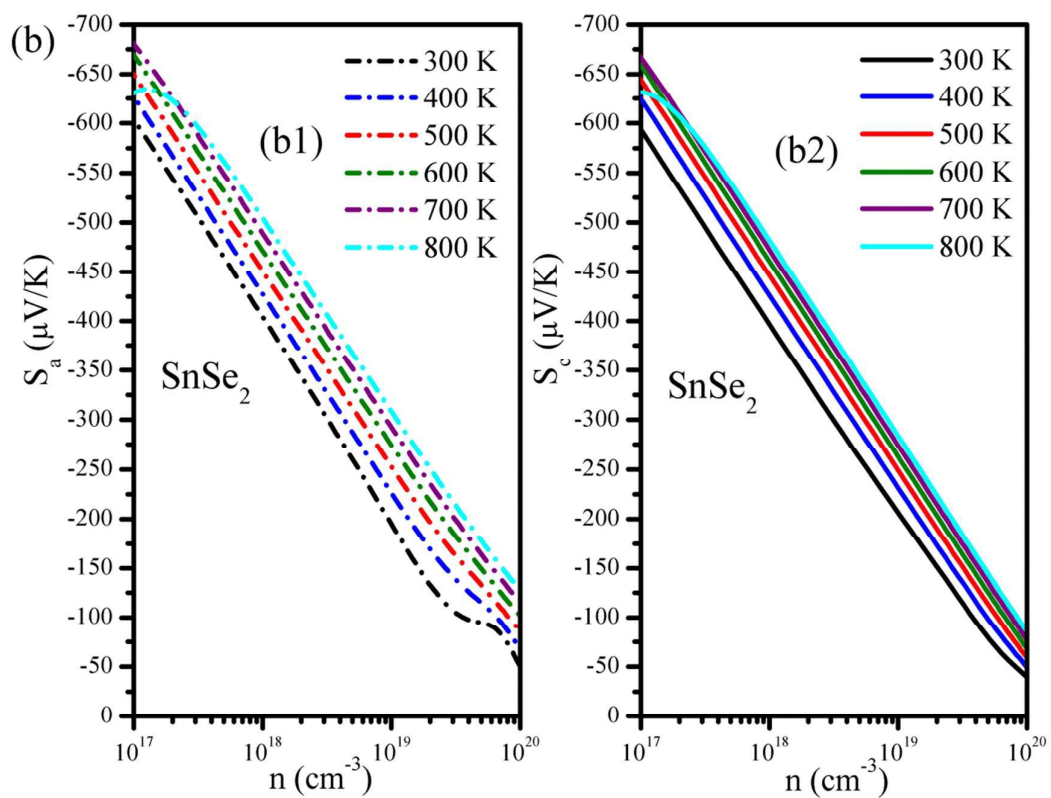
5

### 1 3.3 Thermoelectric properties

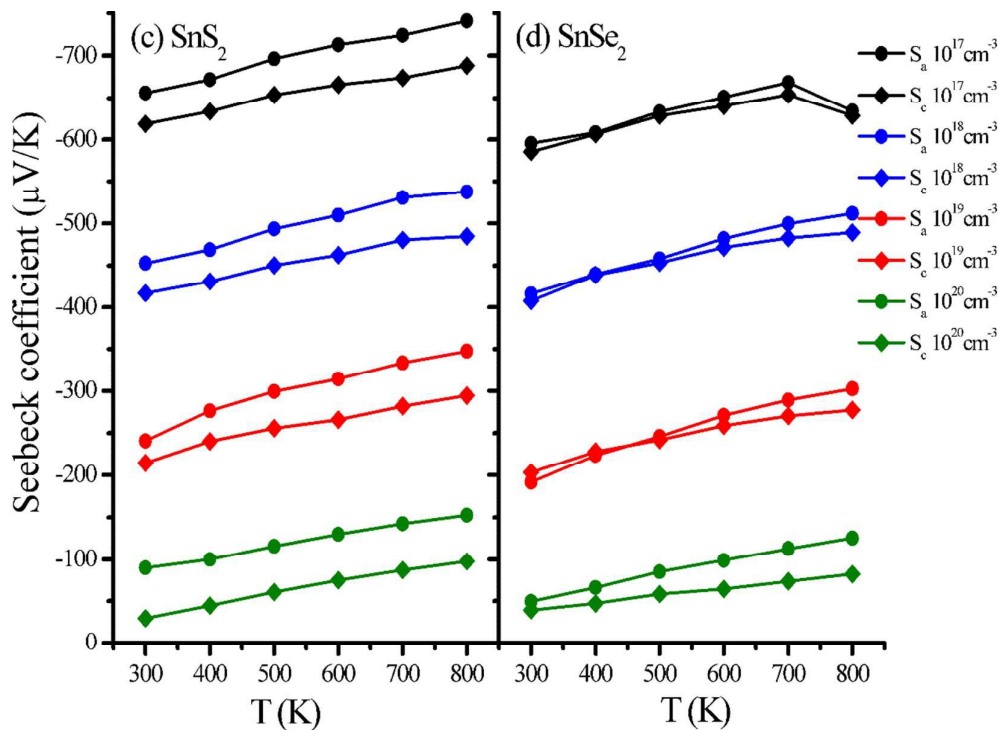
2 Since, as mentioned previously, the anisotropy and anharmonicity is a significant  
3 issue for layered materials. The anisotropic transport properties of SnS<sub>2</sub> and SnSe<sub>2</sub> are  
4 calculated based on the calculated electronic structure using the Boltzmann theory.  
5 The carrier concentration greatly affects  $S$  and  $\sigma$ , so we simulated doping using the  
6 rigid band approximation. The Seebeck coefficients along the  $a$  and  $c$  directions are  
7 shown in Fig. 3. Fig. 3(a) and (c) shows the anisotropy of  $S$  of SnS<sub>2</sub> at different carrier  
8 concentrations and at different temperatures. Clearly, the  $S$  shows a near linear  
9 decrease with increasing carrier concentration but exhibits an increasing trend with  
10 temperature. Also, the values of  $S$  are very different along the  $a$  and  $c$  directions. The  
11 values along the  $a$  direction are larger than those along the  $c$  direction, which  
12 confirms the conclusion obtained from DOS and effective mass analysis. Such  
13 anisotropy is affected by temperature and carrier concentration in different ways (see  
14 Fig. 3(c)). At high carrier concentration, for example, the anisotropy at  $n = 10^{20} \text{ cm}^{-3}$   
15 nearly keeps unchanged with temperature. While at mid-and-low carrier  
16 concentrations, the anisotropy becomes larger and larger with rising temperature.  
17



1



2



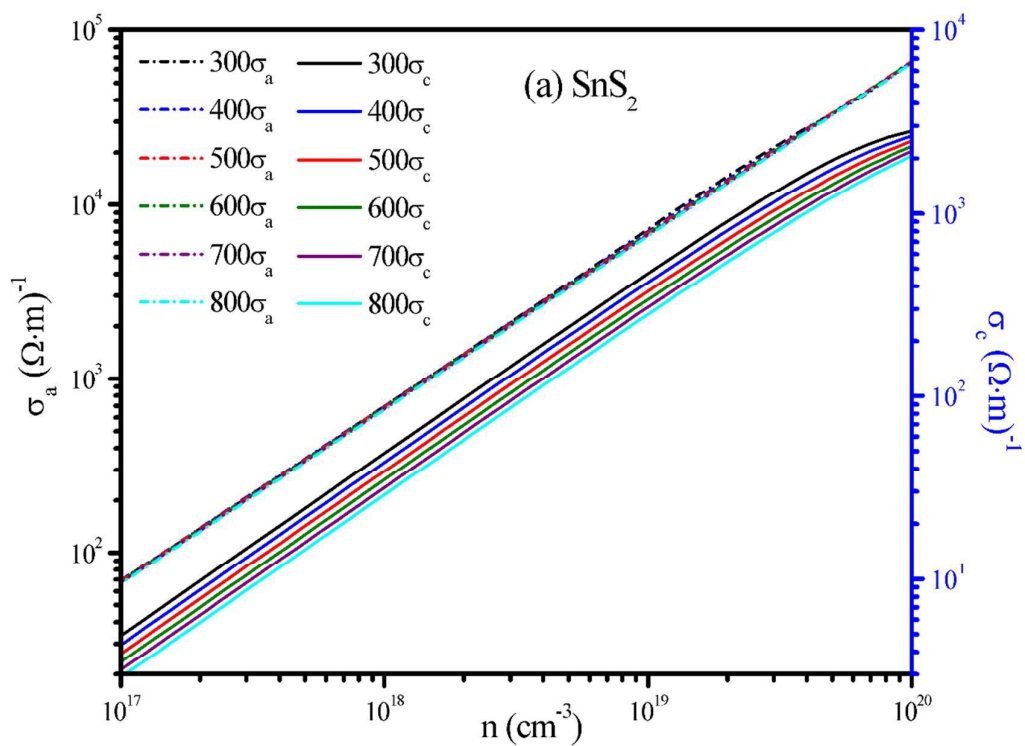
1  
2 **Fig. 3** Seebeck coefficients of SnS<sub>2</sub> and SnSe<sub>2</sub> along the *a* ( $S_a$ ) and *c* ( $S_c$ )  
3 directions as a function of carrier concentration and temperature ranging from  
4 300 K to 800 K.

5  
6 For SnSe<sub>2</sub> (see Fig. 3(b)), due to smaller band gap, the bipolar conduction starts to  
7 play a role below  $\sim 2 \times 10^{17} \text{ cm}^{-3}$  for 800 K and above  $\sim 4 \times 10^{19} \text{ cm}^{-3}$  for 300 K and 400  
8 K. However, they do not enter into the regime of probable optimal doping. Optimal  
9 doping ranges are given as  $8.61 \times 10^{18} - 2.03 \times 10^{19} \text{ cm}^{-3}$  for *a* direction while  
10  $1.71 \times 10^{19} - 2.47 \times 10^{19} \text{ cm}^{-3}$  for *c* direction (see Fig. 7(b)). Therefore, the *ZT* values for  
11 SnSe<sub>2</sub> will not be affected by the bipolar effect in the optimal doping range. The big  
12 difference between SnSe<sub>2</sub> and SnS<sub>2</sub> is that SnSe<sub>2</sub> shows a smaller anisotropy in the  
13 Seebeck coefficient. As seen in Fig. 3(d), at mid-and-low carrier concentration, the  
14 anisotropy almost disappears below 500 K and becomes larger above 500 K. Specially,  
15 the *S* at  $n = 10^{17} \text{ cm}^{-3}$  increases with temperature below 700 K and suddenly turns to

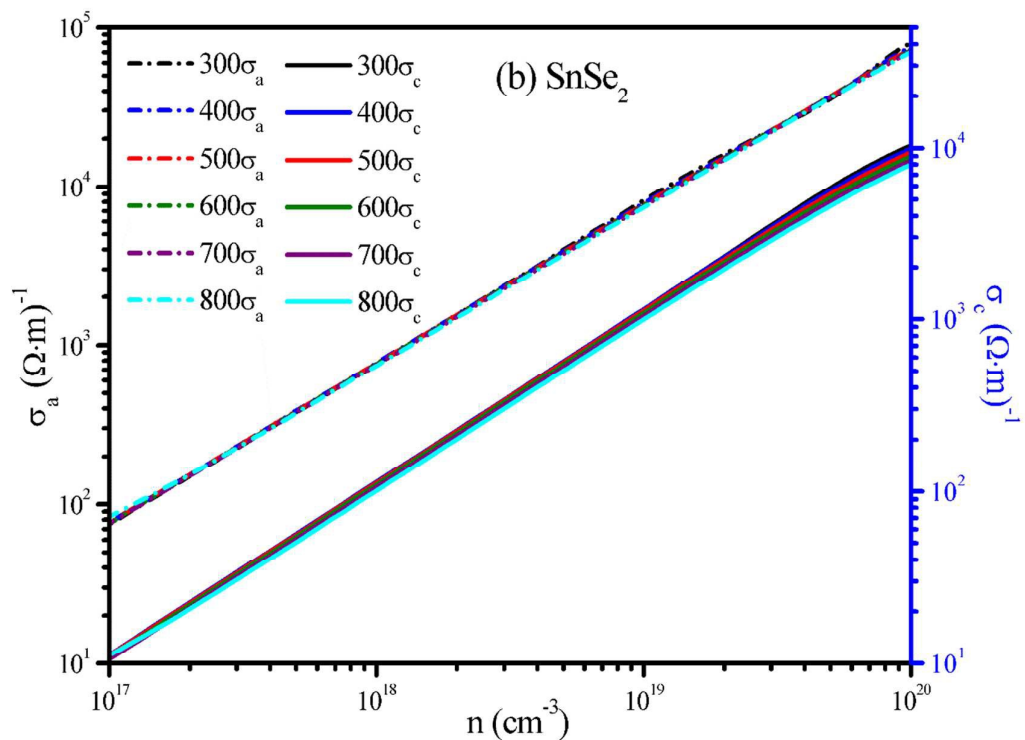
1 decrease at 800 K due to the bipolar effect. At high doping levels, the anisotropy of  $S$   
2 shows an overall increase with increasing temperature up to 800 K.

3 The calculated result  $\sigma/\tau$  includes the scattering rate  $\tau^{-1}$ . To obtain the particular value  
4 of  $\sigma$ , we used the experimental data in ref. 47 to derive the value of  $\tau$ . Comparing the  
5 calculated electrical conductivities (per relaxation time) at room temperature with the  
6 reported experimental conductivities of SnS<sub>2</sub> and SnSe<sub>2</sub> samples ( $2.38 \times 10^{-3}$  and 100  
7  $\Omega^{-1} \cdot \text{m}^{-1}$ ,<sup>51</sup> respectively) yields relaxation times of about 1.37 and 1.28 fs, respectively,  
8 which agree with the typical relaxation time values for semiconductors. We then  
9 calculated  $\sigma$  by  $\sigma/\tau \times \tau$ . For SnS<sub>2</sub>, the calculated  $\sigma$  is  $15.33 \Omega^{-1} \cdot \text{m}^{-1}$  at 300 K and at a  
10 carrier concentration of  $3.2 \times 10^{16} \text{ cm}^{-3}$ . Agreement between calculated value and  
11 experiment ( $16.56 \Omega^{-1} \cdot \text{m}^{-1}$ )<sup>52</sup> is quite good. The resulting electrical conductivities  
12 along the  $a$  and  $c$  directions are shown in Fig. 4. For both materials, the value of  $\sigma$  is  
13 little affected by temperature in both directions. For example, for SnS<sub>2</sub> at  $n = 10^{19}$   
14  $\text{cm}^{-3}$ , the  $\sigma$  along the  $c$  direction reduces slightly from 493.65 to 305.30  $\Omega^{-1} \cdot \text{m}^{-1}$  for  
15 the temperature from 300 K up to 800 K. However, the doping dependence of  $\sigma$  is  
16 more pronounced. The values of  $\sigma$  in both directions increase greatly with the  
17 increase in carrier concentration. Taking SnS<sub>2</sub> as an example, as the carrier  
18 concentration increases from  $10^{17}$  to  $10^{20} \text{ cm}^{-3}$ , the  $\sigma$  at 800 K varies rapidly from  
19 68.38 to  $66.20 \times 10^3 \Omega^{-1} \cdot \text{m}^{-1}$  for  $a$  direction while from 2.97 to  $2.10 \times 10^3 \Omega^{-1} \cdot \text{m}^{-1}$  for  
20  $c$  direction. For SnS<sub>2</sub>, Madelung<sup>53</sup> and Julier<sup>51</sup> also reported that the electrical  
21 conductivities at 300 K increase from  $2.38 \times 10^{-3}$  to  $90 \Omega^{-1} \cdot \text{m}^{-1}$  with carrier  
22 concentrations from  $10^{13}$  to  $2 \times 10^{17} \text{ cm}^{-3}$ .

1



2



3

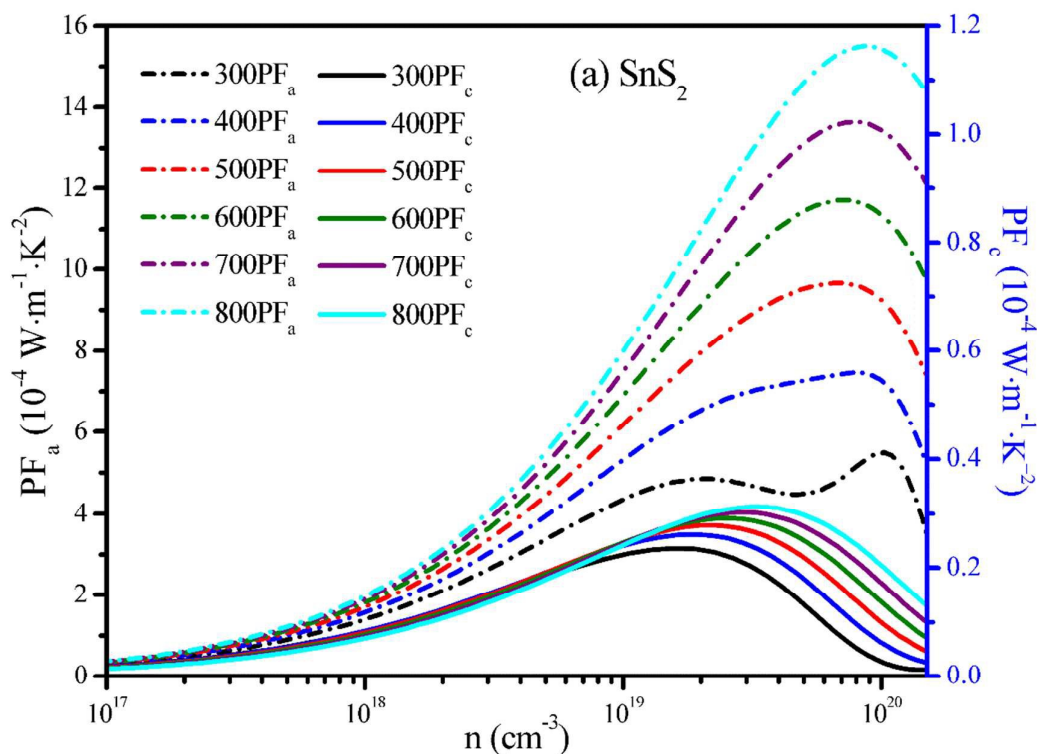
4 **Fig. 4** Electrical conductivities of  $\text{SnS}_2$  and  $\text{SnSe}_2$  along the  $a$  ( $\sigma_a$ ) and  $c$  ( $\sigma_c$ )  
 5 directions as a function of carrier concentration in the temperature range of 300-800  
 6 K.

7

1 Compared to the anisotropy of Seebeck coefficient, the electrical conductivity  
2 anisotropy tends to be larger. At a given temperature and carrier concentration, the  
3 value of  $\sigma$  along the  $a$  direction is much greater than that along the  $c$  direction due to  
4 the weaker interactions between layers in the  $c$  direction. For example, for SnS<sub>2</sub> at  $T =$   
5 300 K and  $n = 10^{19} \text{ cm}^{-3}$ , the  $\sigma$  along the  $a$  and  $c$  directions is  $7.62 \times 10^3$  and  $4.94 \times$   
6  $10^2 \text{ } \Omega^{-1} \cdot \text{m}^{-1}$ , respectively. Experimental measurements<sup>54-56</sup> also showed  $a$  axis is more  
7 conducting than  $c$  axis. The anisotropy ratio  $\sigma_a/\sigma_c$  is found to be greater for SnS<sub>2</sub> than  
8 that for SnSe<sub>2</sub>, which agrees with our results. In our case, it is found that the  
9 anisotropy ratio  $\sigma_a/\sigma_c$  is 12.80 for SnS<sub>2</sub> and 6.92 for SnSe<sub>2</sub> when the carrier  
10 concentration is  $10^{17} \text{ cm}^{-3}$  and the temperature is 300 K. This means SnS<sub>2</sub> has larger  
11 electrical conductivity anisotropy than SnSe<sub>2</sub>. However, the temperature has little  
12 effect on the electrical conductivity anisotropy (see Fig. S2). For SnS<sub>2</sub>, compared with  
13 SnSe<sub>2</sub>, it has lower values of  $\sigma$  but higher Seebeck coefficients in both directions at a  
14 given temperature and carrier concentration. The trend can be explained by the fact  
15 that SnS<sub>2</sub> has larger electron effective masses than SnSe<sub>2</sub> in both directions.

16 Under a given temperature difference, the ability of a material to produce useful  
17 electrical power is quantified by its power factor ( $PF$ ):  $PF = S^2 \sigma$ . We have calculated  
18 this parameter as a function of the carrier concentration and temperature and plotted  
19 the results in Fig. 5. As shown in Fig. 5, for both materials, the  $PF$  along the  $a$   
20 direction is much greater than that along the  $c$  direction. This behavior agrees  
21 reasonably well with the magnitude of  $S$  and  $\sigma$  in  $a$  and  $c$  directions. As a  
22 consequence, the TE properties of SnX<sub>2</sub> are dominated by the  $PF$  along the  $a$

1 direction. In both directions, there is an optimal carrier concentration to yield the peak  
 2  $PF$ , which grows with rising temperature mainly because of larger Seebeck  
 3 coefficient at higher temperature. At 800 K, this parameter along the  $a$  axis reaches  
 4 the values  $15.50 \times 10^{-4}$  and  $11.72 \times 10^{-4} \text{ W}\cdot\text{m}^{-1}\cdot\text{K}^{-2}$  at the carrier concentrations of  $8.59$   
 5  $\times 10^{19}$  and  $7.21 \times 10^{19} \text{ cm}^{-3}$  for  $\text{SnS}_2$  and  $\text{SnSe}_2$ , respectively. Compared to typical TE  
 6 material  $\text{Bi}_2\text{Te}_3$  ( $40 \times 10^{-4} \text{ W}\cdot\text{m}^{-1}\cdot\text{K}^{-2}$  in the  $ab$  plane)<sup>12</sup>, the power factors obtained in  
 7  $\text{SnS}_2$  and  $\text{SnSe}_2$  crystals are lower, but are comparable to those found in other  
 8 thermoelectrics with layered structure (for example,  $\text{SnSe}$ <sup>7</sup> and  $\text{SnS}$ <sup>8,46</sup>). On the other  
 9 hand, Fig. 5 shows that as the temperature increases, the difference of peak  $PF$  values  
 10 between the two directions grows.



11

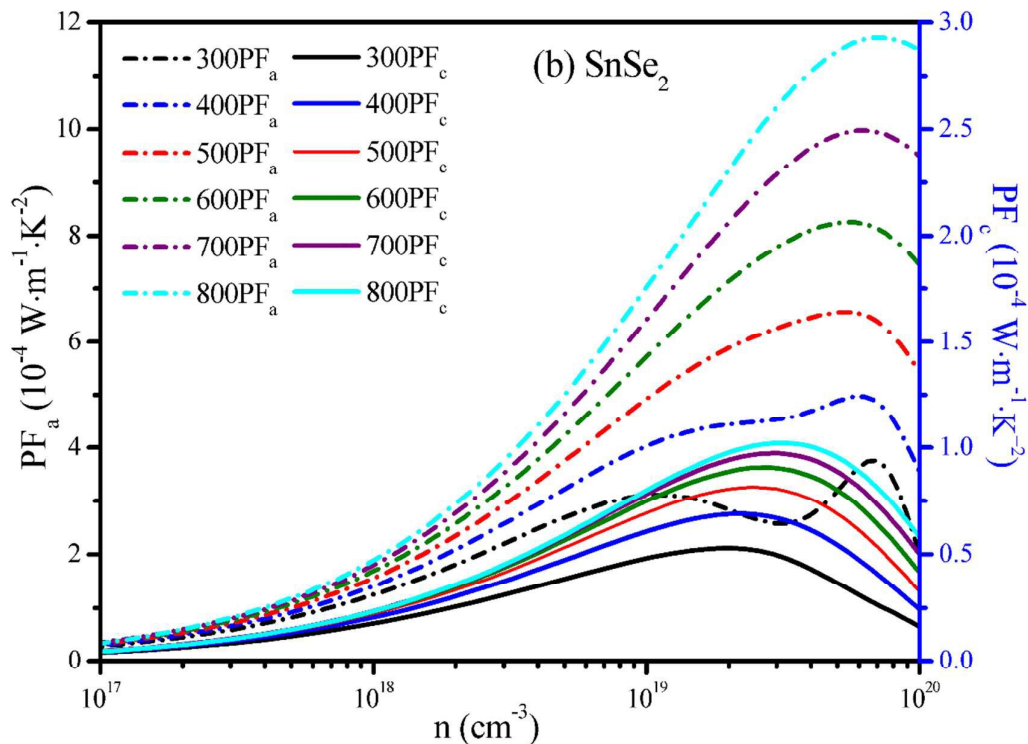


**Fig. 5** Power factors ( $S^2\sigma$ ) of SnS<sub>2</sub> and SnSe<sub>2</sub> along the  $a$  ( $PF_a$ ) and  $c$  ( $PF_c$ ) directions as a function of carrier concentration in the temperature range of 300-800 K.

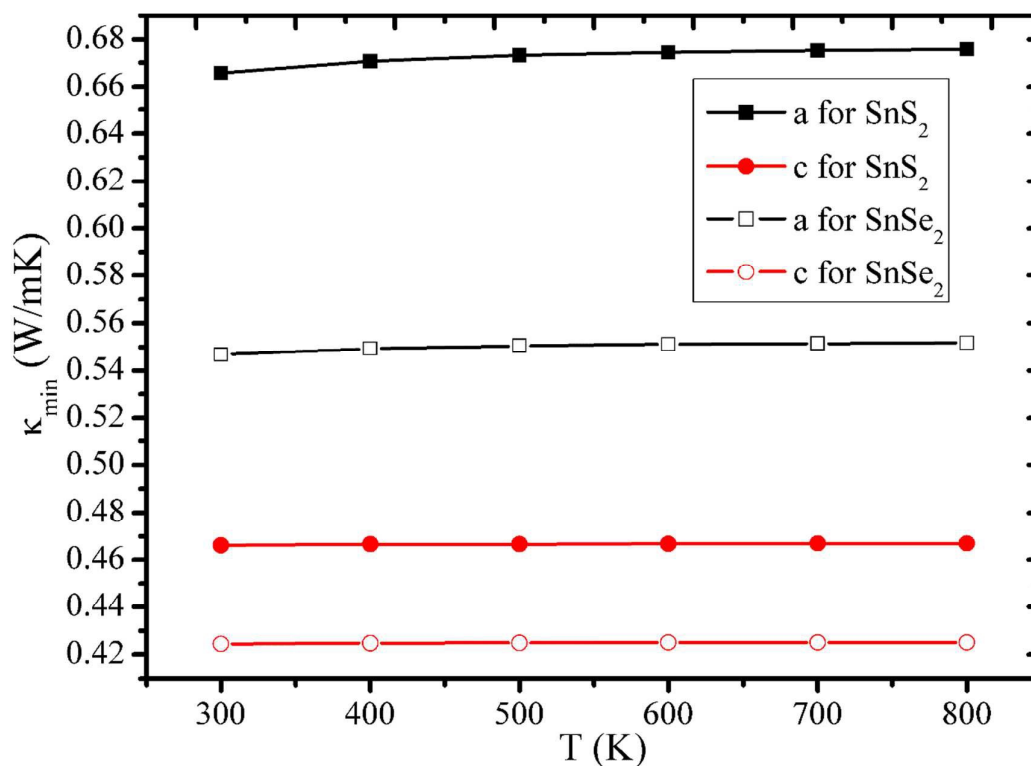
The minimum lattice thermal conductivities can be evaluated using the approach developed by Cahill, as illustrated by Eqs. (2). This model assumes that the conductivity is not limited by phonon-phonon scattering but by a temperature-independent structural scattering mechanism. In this treatment, the predicted thermal conductivity shows a weak temperature-dependence. Because the structures of SnS<sub>2</sub> and SnSe<sub>2</sub> are similar to WSe<sub>2</sub>, it might be more appropriate to calculate the thermal conductivity by the methods used in WSe<sub>2</sub>-type systems. At present, molecular dynamics (MD) simulation and ShengBTE methods are applied to calculate the thermal conductivities of WSe<sub>2</sub>-type systems.<sup>28, 57, 58</sup> However, the approach of MD simulation suffers from problems of low accuracy and lack of

1 transferability, since an appropriate potential for each compound must be developed.  
2 ShengBTE can be applied to pursue the accurate prediction of the lattice thermal  
3 conductivity without any assumption about phonon lifetimes, including the  
4 dependence on the phonon mean free path. The more accurate prediction for thermal  
5 conductivity is favorite. In our next work, we will apply the available computational  
6 code for the prediction of the lattice thermal conductivity. Nevertheless, the minimum  
7 lattice thermal conductivity is an important and useful referenced parameter for  
8 experiments even it might be not able to be fully obtained by the experiments.

9 The temperature-dependent of theoretically predicted minimal lattice thermal  
10 conductivity ( $\kappa_{\min}$ ) of SnS<sub>2</sub> and SnSe<sub>2</sub> is depicted in Fig. 6. For both materials, the  
11 lattice thermal conductivity is obviously anisotropic that the trend of  $\kappa_{\min}$  in the two  
12 directions is always in the order:  $\kappa_{\min}^a > \kappa_{\min}^c$ . Such anisotropy could be attributed to  
13 the anisotropic structures of the two materials. The acoustic modes along the  $G \rightarrow A$   
14 Brillouin zone direction ( $c$  axis) are significantly softer (with lower Debye  
15 temperatures and smaller phonon velocities; see Fig. S3 and Table S1) than those  
16 along  $G \rightarrow K$  Brillouin zone direction ( $a$  axis). These softer modes along the  $c$  axis  
17 lead to smaller lattice thermal conductivity in this direction. For both directions,  
18 SnSe<sub>2</sub> has lower values of  $\kappa_{\min}$  than SnS<sub>2</sub>, also determined by softer acoustic modes in  
19 SnSe<sub>2</sub> than in SnS<sub>2</sub>. Similar trend is also found in a comparison between SnSe and  
20 SnS. At 300 K, for SnS<sub>2</sub>, the values of  $\kappa_{\min}$  are (in  $\text{W}\cdot\text{m}^{-1}\cdot\text{K}^{-1}$ )  $\sim 0.67$  and  $\sim 0.47$  along  
21 the  $a$  and  $c$  axis directions, respectively; for SnSe<sub>2</sub>, the values decrease separately to  
22 0.55 and 0.42  $\text{W}\cdot\text{m}^{-1}\cdot\text{K}^{-1}$ . Unfortunately, we cannot find the corresponding

1 experimental data for a comparison. However, these values are comparable to the  
 2 measured  $\kappa_L$  in SnSe (about  $0.7 \text{ W}\cdot\text{m}^{-1}\cdot\text{K}^{-1}$  at 300 K)<sup>7</sup> and even lower than that in  
 3  $\text{Bi}_2\text{Te}_3$  (about  $1.28 \text{ W}\cdot\text{m}^{-1}\cdot\text{K}^{-1}$  at 300 K)<sup>59</sup>. For both  $\text{SnS}_2$  and  $\text{SnSe}_2$ , the  $\kappa_{\min}$  increases  
 4 slowly with increasing temperature along the  $a$  direction whereas almost hold the  
 5 same values along the  $c$  directions. Considering  $\text{SnX}_2$  possesses large power factor  
 6 and low thermal conductivity,  $\text{SnX}_2$  may serve as a new potential candidate for TE  
 7 applications.

8



9

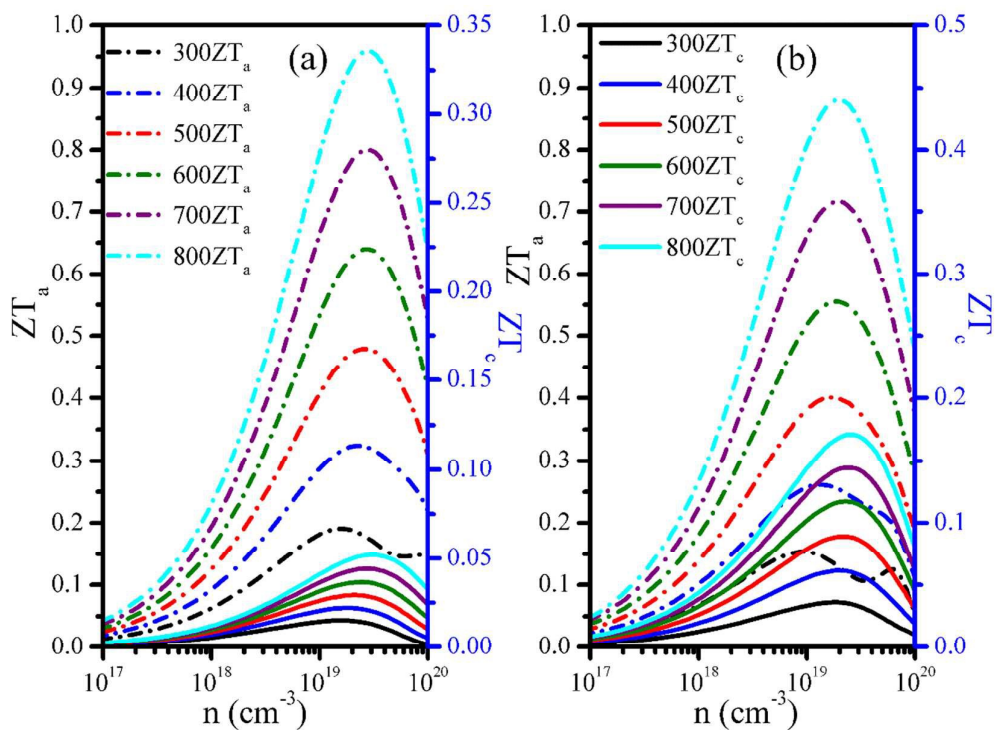
10 **Fig. 6** Calculated minimum lattice thermal conductivities for  $a$  and  $c$  directions in  
 11  $\text{SnX}_2$  ( $X = \text{S}, \text{Se}$ ) as a function of temperature ranging from 300 K to 800 K.

12

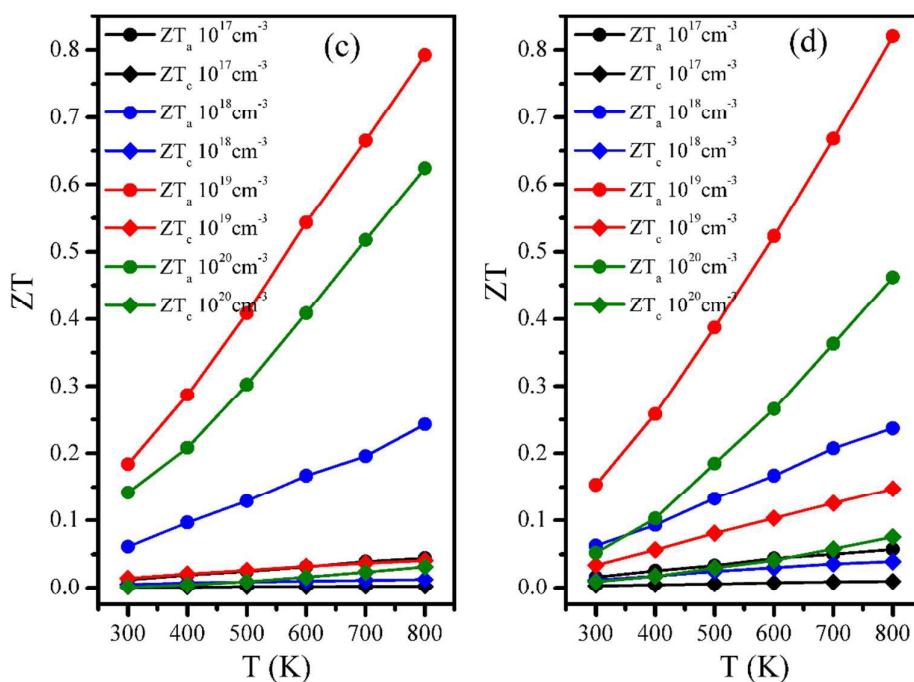
13 Using the above calculated minimum lattice thermal conductivity of  $\text{SnX}_2$ , we

14 were able to make an estimate of  $ZT$  (see Fig. 7). Fig. 7(a) and (b) shows the

1 dependence of  $ZT$  on the carrier concentration for  $\text{SnS}_2$  and  $\text{SnSe}_2$ . The anisotropy of  
2  $S$ ,  $\sigma$ ,  $\kappa_E$  and  $\kappa_L$  in  $\text{SnX}_2$  crystals inevitably results in the anisotropy of  $ZT$ . Indeed,  $ZT$   
3 exhibits a strong anisotropy for both materials. As mentioned above, the electronic  
4 conductivity along the  $a$  axis can be substantially greater than that along the  $c$  axis.  
5 This is enough to compensate for a lattice thermal conductivity along the  $c$  axis that is  
6 about  $0.2 \text{ W}\cdot\text{m}^{-1}\cdot\text{K}^{-1}$  lower than that along the  $a$  axis. It induces remarkably higher  $ZT$   
7 values in the  $a$  direction. In Fig. 7(a) and (b) it is easily found that the  $ZT$  value can be  
8 highly influenced by carrier concentration. The  $ZT$  value first increases with the  
9 carrier concentration, reaches an optimal value, and then decreases. For  $\text{SnS}_2$ , the  
10 peak  $ZT$  value increases from 0.19 to 0.96 along the  $a$  axis while rises from 0.02 to  
11 0.05 along the  $c$  axis for temperature from 300 K up to 800 K. For  $\text{SnSe}_2$ , compared  
12 with  $\text{SnS}_2$ , the optimal  $ZT$  value is slightly lower in the  $a$  direction whereas slightly  
13 higher in the  $c$  direction, which ranges from 0.15 to 0.88 for the former and varies  
14 from 0.04 to 0.17 for the latter in the 300-800 K temperature range. The  $ZT$  values  
15 along the  $c$  axis are much lower than those along the  $a$  axis, in particularly for  $\text{SnS}_2$ .  
16 Therefore,  $a$  direction of both materials is a preferred direction for TE application. In  
17 the preferred direction, the highest peak  $ZT$  value is predicted to be 0.96 for  $\text{SnS}_2$  and  
18 0.88 for  $\text{SnSe}_2$  when  $n = 2.87 \times 10^{19} \text{ cm}^{-3}$  and  $n = 1.94 \times 10^{19} \text{ cm}^{-3}$ , respectively. Such  
19 doping concentration is probably experimentally controllable.



1



2

3 **Fig. 7** (a) and (b):  $ZT$  values for  $a$  ( $ZT_a$ ) and  $c$  ( $ZT_c$ ) directions in  $\text{SnX}_2$  as a function of  
 4 carrier concentration, (a) is for  $\text{SnS}_2$  and (b) for  $\text{SnSe}_2$ ; (c) and (d):  $ZT$  values for  $a$   
 5 ( $ZT_a$ ) and  $c$  ( $ZT_c$ ) directions in  $\text{SnX}_2$  as a function of temperature ranging from 300 to  
 6 800 K, (c) is for  $\text{SnS}_2$  and (d) for  $\text{SnSe}_2$ .

7

1 The temperature dependence of  $ZT$  for  $\text{SnS}_2$  and  $\text{SnSe}_2$  at four different carrier  
2 concentrations i.e.  $10^{17}$ ,  $10^{18}$ ,  $10^{19}$  and  $10^{20} \text{ cm}^{-3}$ , respectively, is plotted in Fig. 7(c)  
3 and (d). As shown in Fig. 7(c) and (d), at the same carrier concentration, the  $ZT$  values  
4 for both materials in both directions exhibit a linear climb as temperature increases in  
5 the 300-800 K temperature range. For example, the  $ZT$  value of  $\text{SnS}_2$  at  $n = 10^{19} \text{ cm}^{-3}$   
6 increases from 0.18 for 300 K to 0.79 for 800 K. Also, its anisotropy becomes  
7 stronger and stronger with temperature. Most interestingly, as temperature increases,  
8 the  $ZT$  and its anisotropy increases at a faster rate at mid carrier concentration and a  
9 slower rate at high carrier concentration. For instance, the  $ZT$  value at  $n = 10^{19} \text{ cm}^{-3}$   
10 increases faster with temperature than that at  $n = 10^{20} \text{ cm}^{-3}$ . All above-mentioned  
11 results undoubtedly reveal that the  $ZT$  value for  $\text{SnX}_2$  compound can be improved by  
12 tuning temperature and carrier concentration.

13 The predicted  $ZT$  values in  $\text{SnX}_2$  are comparable to that of the commercial TE  
14 material  $\text{Bi}_2\text{Te}_3$  (about 0.8). Compared with reported  $\text{MX}_2$  compounds, the  $ZT$  value  
15 in  $\text{SnX}_2$  is remarkably lower than those found in  $n$ -type 1TL- $\text{MoS}_2$  and 2TL- $\text{WSe}_2$   
16 (about 1.6 and 2.1, respectively<sup>60</sup>) but higher than other  $\text{MX}_2$  compounds such as  $\text{TiS}_2$ ,  
17  $\text{TiSe}_2$ , and  $\text{ZrSe}_2$ . For example, The  $ZT$  reaches a maximum value of 0.54 at 700 K for  
18  $\text{Cu}_{0.05}\text{TiS}_{1.5}\text{Se}_{0.5}$ , the highest value so far observed in layered titanium  
19 chalcogenides.<sup>27</sup> However, the best  $ZT$  value is only 0.25 for Li-intercalated  $\text{ZrSe}_2$ .<sup>61</sup>

## 20 Conclusions

21 In conclusion, we have systematically investigated the crystal structure, electronic  
22 structure and anisotropic thermoelectric properties of  $\text{SnX}_2$  ( $X = \text{S}$  or  $\text{Se}$ ) via

1 first-principles method. The results reveal that the anisotropic structure of layered  
2  $\text{SnX}_2$  compound brings about the anisotropy of transport coefficients, which behaves  
3 in different ways. For  $\text{SnS}_2$ , the anisotropy of Seebeck coefficient is little affected by  
4 temperature at high carrier concentration whereas becomes larger and larger at  
5 mid-and-low carrier concentrations. For  $\text{SnSe}_2$ , differently, at high doping levels, the  
6 Seebeck coefficient anisotropy shows an overall increase with increasing temperature  
7 up to 800 K. At mid-and-low carrier concentration, it almost disappears below 500 K  
8 and tends to be higher above 500 K. Our calculations also suggest the temperature has  
9 little effect on the electrical conductivity and hence its anisotropy. The remarkably  
10 greater electrical conductivity in the  $a$  direction along with the corresponding higher  
11 Seebeck coefficient induces larger power factor in this direction. In the  $a$  direction,  
12 the peak  $PF$  can reach  $15.50 \times 10^{-4}$  and  $11.72 \times 10^{-4} \text{ W}\cdot\text{m}^{-1}\cdot\text{K}^{-2}$  for  $\text{SnS}_2$  and  $\text{SnSe}_2$ ,  
13 respectively. The values are almost equal to those found in  $\text{SnSe}$  and  $\text{SnS}$ . At 300 K,  
14 the predicted minimum lattice thermal conductivities along the  $a$  axis are (in  
15  $\text{W}\cdot\text{m}^{-1}\cdot\text{K}^{-1}$ ) about 0.67 and 0.55 for  $\text{SnS}_2$  and  $\text{SnSe}_2$ , respectively. Moreover, for both  
16 materials, the parameter only increases slowly with temperature. The large peak  $PF$   
17 and low lattice thermal conductivity are favorable for producing good thermoelectric  
18 performance along the  $a$  direction. In this direction,  $\text{SnSe}_2$  can show a peak  $ZT$  value  
19 of 0.88 at 800 K when the carrier concentration reaches  $1.94 \times 10^{19} \text{ cm}^{-3}$ . For  $\text{SnS}_2$ , an  
20 even higher  $ZT$  value of 0.96 can be obtained at the same temperature when the carrier  
21 concentration approaches  $2.87 \times 10^{19} \text{ cm}^{-3}$ . The values of this parameter in  $\text{SnX}_2$  ( $X =$   
22 S, Se) are comparable to the typical  $ZT$  values 0.8 of  $\text{Bi}_2\text{Te}_3$ . Therefore, these layered

1 metal dichalcogenides would have promising prospects for thermoelectric  
2 applications. Further deeper theoretical and experimental studies are required to  
3 explore this class of materials.

4

## 5 **Acknowledgments**

6 This work was supported by the China Postdoctoral Science Foundation  
7 (2014M551848), NSFC project (No: 21303025 and 91122015). B.-Z. Sun thanks the  
8 support from the Natural Science Foundation of Guangxi province  
9 (2014GXNSFBA118029), and the Scientific Research Foundation of Guangxi  
10 University (XBZ120059).

11

## 12 **Notes and references**

- 13 1. F. J. DiSalvo, *Science*, 1999, **285**, 703-706.
- 14 2. L. E. Bell, *Science*, 2008, **321**, 1457-1461.
- 15 3. M. W. Gaultois, T. D. Sparks, C. K. H. Borg, R. Seshadri, W. D. Bonificio and D. R.  
16 Clarke, *Chem Mater*, 2013, **25**, 2911-2920.
- 17 4. D. Parker and D. J. Singh, *Phys Rev X*, 2011, **1**.
- 18 5. X. Yan, B. Poudel, Y. Ma, W. S. Liu, G. Joshi, H. Wang, Y. Lan, D. Wang, G. Chen and Z.  
19 F. Ren, *Nano Lett*, 2010, **10**, 3373-3378.
- 20 6. X. Tang, W. Xie, H. Li, W. Zhao, Q. Zhang and M. Niino, *Appl Phys Lett*, 2007, **90**,  
21 012102.
- 22 7. L. D. Zhao, S. H. Lo, Y. Zhang, H. Sun, G. Tan, C. Uher, C. Wolverton, V. P. Dravid and  
23 M. G. Kanatzidis, *Nature*, 2014, **508**, 373-377.

- 1 8. Q. Tan, L. D. Zhao, J. F. Li, C. F. Wu, T. R. Wei, Z. B. Xing and M. G. Kanatzidis, *J*  
2 *Mater Chem A*, 2014, **2**, 17302-17306.
- 3 9. J. M. Skelton, S. C. Parker, A. Togo, I. Tanaka and A. Walsh, *Phys Rev B*, 2014, **89**.
- 4 10. H. Wang, Y. Pei, A. D. LaLonde and G. J. Snyder, *Adv Mater*, 2011, **23**, 1366-1370.
- 5 11. M. Lee, L. Viciu, L. Li, Y. Wang, M. L. Foo, S. Watauchi, R. A. Pascal Jr, R. J. Cava and  
6 N. P. Ong, *Nat Mater*, 2006, **5**, 537-540.
- 7 12. I. Terasaki, Y. Sasago and K. Uchinokura, *Phys Rev B*, 1997, **56**, R12685-R12687.
- 8 13. F. Ryoji, M. Ichiro, I. Hiroshi, T. Tsunehiro, M. Uichiro and S. Satoshi, *Jpn J Appl Phys*,  
9 2000, **39**, L1127.
- 10 14. W. Xie, J. He, H. J. Kang, X. Tang, S. Zhu, M. Laver, S. Wang, J. R. D. Copley, C. M.  
11 Brown, Q. Zhang and T. M. Tritt, *Nano Lett*, 2010, **10**, 3283-3289.
- 12 15. K. Takahata, Y. Iguchi, D. Tanaka, T. Itoh and I. Terasaki, *Phys Rev B*, 2000, **61**, 12551.
- 13 16. M. Antoine, G. Emmanuel, G. Franck, B. Yohann and H. Vincent, *Sci Technol Adv Mater*,  
14 2012, **13**, 053003.
- 15 17. J. Carrete, N. Mingo and S. Curtarolo, *Appl Phys Lett*, 2014, **105**, 101907.
- 16 18. J. Wilson and A. Yoffe, *Adv Phys*, 1969, **18**, 193-335.
- 17 19. K. Rossnagel, *J Phys: Condens Matter*, 2011, **23**, 213001.
- 18 20. L. Rapoport, N. Fleischer and R. Tenne, *J Mater Chem*, 2005, **15**, 1782-1788.
- 19 21. A. V. Kuranov, V. G. Pleshchev, A. N. Titov, N. V. Baranov and L. S. Krasavin, *Phys*  
20 *Solid State*, 2000, **42**, 2089-2092.
- 21 22. F. Gascoin, N. Raghavendra, E. Guilmeau and Y. Bréard, *J Alloy Compd*, 2012, **521**,  
22 121-125.

- 1 23. S. Hébert, W. Kobayashi, H. Muguerra, Y. Bréard, N. Raghavendra, F. Gascoin, E.  
2 Guilmeau and A. Maignan, *Phys Status Solidi A*, 2013, **210**, 69-81.
- 3 24. E. Guilmeau, Y. Bréard and A. Maignan, *Appl Phys Lett*, 2011, **99**, 052107.
- 4 25. X. Huang, Z. Zeng and H. Zhang, *Chem Soc Rev*, 2013, **42**, 1934-1946.
- 5 26. C. Lee, J. Hong, M.-H. Whangbo and J. H. Shim, *Chem Mater*, 2013, **25**, 3745-3752.
- 6 27. R. Nunna, F. Gascoin and E. Guilmeau, *J Alloy Compd*, 2015, **634**, 32-36.
- 7 28. A. N. Gandhi and U. Schwingenschlögl, *Chem Mater*, 2014, **26**, 6628-6637.
- 8 29. T. M. Tritt and M. A. Subramanian, *Mrs Bull*, 2006, **31**, 188-198.
- 9 30. A. A. Kozma, M. Y. Sabov, E. Y. Peresh, I. E. Barchiy and V. V. Tsygyka, *Inorg Mater*,  
10 2015, **51**, 93-97.
- 11 31. I. O. Nasibov, T. I. Sultanov, P. G. Rustamov and M. A. Alidzhanov, *Izv. Akad. Nauk*  
12 *SSSR, Neorg. Mater.*, 1977, **13**, 982-985.
- 13 32. G. K. H. Madsen and D. J. Singh, *Comput Phys Commun*, 2006, **175**, 67-71.
- 14 33. D. Cahill, S. Watson and R. Pohl, *Phys Rev B*, 1992, **46**, 6131-6140.
- 15 34. G. Kresse and J. Furthmüller, *Phys Rev B*, 1996, **54**, 11169-11186.
- 16 35. J. Heyd, G. E. Scuseria and M. Ernzerhof, *J Chem Phys*, 2003, **118**, 8207-8215.
- 17 36. M.-S. Lee and S. D. Mahanti, *Phys Rev B*, 2012, **85**, 165149.
- 18 37. Y. Wang, X. Chen, T. Cui, Y. Niu, Y. Wang, M. Wang, Y. Ma and G. Zou, *Phys Rev B*,  
19 2007, **76**, 155127.
- 20 38. V. K. Gudelli, V. Kanchana, S. Appalakondaiah, G. Vaitheeswaran and M. C. Valsakumar,  
21 *J Phys Chem C*, 2013, **117**, 21120-21131.
- 22 39. C. Wang, Y. Wang, G. Zhang and C. Peng, *J Phys Chem C*, 2013, **117**, 21037-21042.

- 1 40. G. Ren, J. Lan, C. Zeng, Y. Liu, B. Zhan, S. Butt, Y.-H. Lin and C.-W. Nan, *JOM*, 2015,  
2 67, 211-221.
- 3 41. J. Lan, Y.-H. Lin, Y. Liu, S. Xu and C.-W. Nan, *J Am Ceram Soc*, 2012, 95, 2465-2469.
- 4 42. S. Baroni, S. de Gironcoli, A. Dal Corso and P. Giannozzi, *Rev Mod Phys*, 2001, 73,  
5 515~562.
- 6 43. A. Togo, F. Oba and I. Tanaka, *Phys Rev B*, 2008, 78, 134106.
- 7 44. R. S. Mitchell, Y. Fujiki and Y. Ishizawa, *Nature*, 1974, 247, 537-538.
- 8 45. J. Robertson, *J Phys C: Solid State Phys*, 1979, 12, 4753.
- 9 46. Q. Tan and J. F. Li, *J Electron Mater*, 2014, 43, 2435-2439.
- 10 47. G. Domingo, R. S. Itoga and C. R. Kannewurf, *Phys Rev*, 1966, 143, 536-541.
- 11 48. P. Lee and G. Said, *J Phys D: Appl Phys*, 1968, 1, 837.
- 12 49. C. Xia, Y. Peng, H. Zhang, T. Wang, S. Wei and Y. Jia, *Phys Chem Chem Phys*, 2014, 16,  
13 19674-19680.
- 14 50. B. L. Evans and R. A. Hazelwood, *J Phys D: Appl Phys*, 1969, 2, 1507.
- 15 51. C. Julien, M. Eddrief, I. Samaras and M. Balkanski, *Mater Sci Eng B*, 1992, 15, 70-72.
- 16 52. L. Sharp, D. Soltz and B. A. Parkinson, *Cryst Growth Des*, 2006, 6, 1523-1527.
- 17 53. O. Madelung, *Semiconductors: Data Handbook*, Springer, New York, 2004.
- 18 54. S. G. Patil and R. H. Tredgold, *J Phys D: Appl Phys*, 1971, 4, 718-722.
- 19 55. M. K. Agarwal, P. D. Patel and S. S. Patel, *J Cryst Growth*, 1991, 110, 553-558.
- 20 56. L. A. Burton, D. Colombara, R. D. Abellon, F. C. Grozema, L. M. Peter, T. J. Savenije, G.  
21 Dennler and A. Walsh, *Chem Mater*, 2013, 25, 4908-4916.
- 22 57. C. Chiritescu, D. G. Cahill, N. Nguyen, D. Johnson, A. Bodapati, P. Keblinski and P.

- 1 Zschack, *Science*, 2007, **315**, 351-353.
- 2 58. S. Kumar and U. Schwingenschlögl, *Chem Mater*, 2015, **27**, 1278-1284.
- 3 59. H. Goldsmid, *Proc Phys Soc B*, 1956, **69**, 203.
- 4 60. W. Huang, X. Luo, C. K. Gan, S. Y. Quek and G. Liang, *Phys Chem Chem Phys*, 2014,
- 5 **16**, 10866-10874.
- 6 61. T. Holgate, Y. Liu, D. Hitchcock, T. Tritt and J. He, *J Electron Mater*, 2013, **42**,
- 7 1751-1755.
- 8
- 9